Science of the Total Environment 907 (2024) 167927

Contents lists available at ScienceDirect

Science of the Total Environment

journal homepage: www.elsevier.com/locate/scitotenv

Non-invasive 3D analysis of microplastic particles in sandy soil — Exploring feasible options and capabilities

Christian Tötzke [a,b,*], Boyana Kozhuharova [a], Nikolay Kardjilov [b], Nicolas Lenoir [c,d], Ingo Manke [b], Sascha E. Oswald [a]

[a] Institute of Environmental Science and Geography, University of Potsdam, Potsdam, Germany
[b] Department for Electrochemical Energy Storage, Helmholtz-Zentrum Berlin für Materialien und Energie, Berlin, Germany
[c] Institut Laue-Langevin, Grenoble, France
[d] Laboratoire 3SR, Université Grenoble Alpes, France

HIGHLIGHTS

- Non-invasive localization of microplas.cs in sandy soil by tomography
- 3D analysis of microplastics particle size and distribution
- 3D study of microplastic effects on soil microstructure
- Detection of microplastic particles in spatial context of plant-soil interactions

GRAPHICAL ABSTRACT

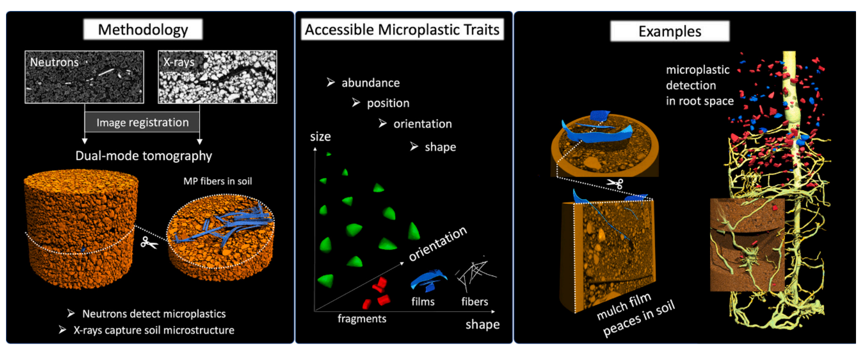

ARTICLE INFO

Editor: Kevin V. Thomas

Keywords:
Non-destructive microplastic detection
Microplastic effects on soil microstructure
Microplastic shape analysis
Mapping 3D soil structure
Neutron tomography
X-ray tomography

ABSTRACT

Increasingly, environmental research efforts seek to understand how the continuous input of microplastics into terrestrial environments alters soil physicochemical properties and affects plants and other soil biota. However, fundamental understanding is hampered by the destructive nature of current analytical techniques, which typically require the disruption of soil samples and often the removal of soil organic matter. This results in the irretrievable loss of essential information about soil microstructure and the spatial distribution of microplastic particles. We showed that the non-invasive approach of dual neutron and X-ray tomography is capable of detecting and localizing microplastics embedded in soil environments with organic components, here tested with peat, charcoal, and bark mulch additions. We explored how the number of microplastic particles can be determined on intact samples, even accompanied by add-on information on the size, shape and distribution of microplastic particles. For some combinations of plastic types and organic material amendments, the basic approach was not successful, but could be enhanced by soaking the sample in hydrogen peroxide solution while largely preserving the integrity of the microstructure, or by including shape parameters into the image analysis. By segmenting images using region growing, we were able to identify all microplastic particles without false positives, even in the presence of organic material. We also succeeded in analyzing small-sized microplastic

* Corresponding author at: Institute of Environmental Science and Geography, University of Potsdam, Potsdam, Germany.
E-mail address: toetzke@uni-potsdam.de (C. Tötzke).

https://doi.org/10.1016/j.scitotenv.2023.167927
Received 30 June 2023; Received in revised form 12 October 2023; Accepted 16 October 2023
Available online 24 October 2023

particles, such as film or fibers, embedded in natural sandy soil. 3D visualization of plastic film fragments together with the soil matrix made it obvious that larger fragments can have a significant impact on soil hydraulic properties. It has also been shown that a group of microplastic fibers can induce a planar crack in the soil matrix. Finally, roots and microplastics could be differentiated and visualized in a soil sample, demonstrating the leeway for the non-invasive study of potential interactions between roots and microplastics.

1. Introduction

A wide range of inexpensive and versatile plastic materials has enabled the mass production of affordable consumer goods in the last decades, leading to a massive increase in the number and types of plastic items used in everyday life, including vast quantities of disposable packaging. The downside of this socio-economic success story, however, is that microplastics have become a ubiquitous pollutant (Rochman, 2018). While plastic contamination of oceans and then other aquatic ecosystems has already been acknowledged as environmental issue for well over a decade, the effects of microplastics (MP) in terrestrial ecosystems have moved into focus of research just comparatively recently (Rillig and Lehmann, 2020). Sources of MP in soils are littering, atmospheric deposition, irrigation and flooding, agricultural mulching and application of compost and sewage sludge (Yu and Flury, 2021). Once these particles have arrived at the soil surface, management practices (Weber et al., 2022), bioturbation (Huerta Lwanga et al., 2017; Rillig et al., 2017) or water percolation (Lwanga et al., 2022; Munz et al., 2023b) contribute to the relocation of microplastics down to considerable depths, where they persist likely for decades or even centuries. Microplastics have been shown to affect various soil properties such as bulk density, contact angle, water holding capacity (Guo et al., 2022; Wang et al., 2023), rate of soil water evaporation (Wan et al., 2019) and the functional relationship between the microbial activity and water stable aggregates (de Souza Machado et al., 2018). The effects of MPs on soil properties and processes appears often conveyed by physical parameters such as shape and size of particles rather than direct chemical toxicity (Rillig and Lehmann, 2020), though MP can also act as carrier of other pollutants that may be released from them (Tang et al., 2021). MP particles more dissimilar in shape to the typical shape of naturally occurring soil particles are thought to have substantial effects on biophysical properties of soil (Rillig et al., 2019). In causing changes in the soil habitat, MP represent a potential threat for soil biota and a risk for food security if entering the food chain (Bläsing and Amelung, 2018).

The effects of MP on plant performance are still largely unclear. In experimental studies, different effects on plant growth have been observed: positive, neutral as well as negative effects. de Souza Machado et al. (2019) showed that higher concentrations of MPs in the soil increased the belowground biomass of spring onions, with the most pronounced effect observed for polyester fibers, whose linear shape, size and flexibility are very different from most natural components of the soil. In another study, the presence of low density polyethylene particles in sandy soil at concentrations above 1 wt% had a positive effect on the growth performance of common beans while the addition of a biodegradable microplastics resulted in significantly lower biomass production (Meng et al., 2021). Decades of mulching practices can lead to massive contamination of agricultural soil with film residue (Huang et al., 2020), which can affect the soil structure hydraulics (Wan et al., 2019). Qi et al. (2018) reported that starch-based biodegradable plastic mulch showed stronger negative effects on wheat growth compared to low density polyethylene. In another experiment, plastic film fragments were shown to have more negative effects on soil water content at low water availability, but positive effects on plant growth were observed with increasing concentration (Krehl et al., 2022). The mentioned studies analyzed the impact of microplastics on plant performance for different soils that contained particles in various concentrations, plastic types, particle shapes and sizes. Such studies generally work with high or extremely high loads of microplastics, because effects on plants are then more easily to identify by statistical analysis. However, often such studies do not allow for directly identifying the underlying processes and may not be able to observe also more subtle effects of MP at smaller environmentally relevant concentrations (Yu et al., 2023). To gain a better mechanistic understanding of how microplastics influence soil properties and how this affects plant performance, studies are required that provide spatially resolved information about the MP distribution in soil including an assessment of the local soil microstructure surrounding the plastic particles.

In recent years, various methods have been developed to detect and analyze microplastics in soil samples. Depending on the objective of the study optical inspection spectroscopic, thermoanalytical or chemical methods are used to analyze specific traits of microplastic pollutants such as abundance, shape, size, type or additives. But all of these methods are based on destructive sampling or involve destructive sample processing, see e.g. the review by Prata et al. (2019). This means that essential information about soil microstructure and the spatial distribution of MP is inevitably lost during the analysis, making it impossible to directly study the impact of the plastic particles on the local microstructure of the soil. Also, fragile MP may be further fragmented during processing or existing fragments of a particle or foil displaced and then only recognized as seemingly separate individuals. An elegant way to get around this problem is to use non-invasive imaging methods that preserve the integrity of the sample structure, useful for time-resolved investigations, analyzing undisturbed cores or relating microplastic position to its local environment. This could be used for concluding on past deposition in sediments or soils (Tötzke et al., 2021b; Weber and Lechthaler, 2021), study microplastic relocation processes, the impact on the pore structure of soil (Xu et al., 2020) or the response of root growth on the presence microplastics. Recently, we presented a combination of neutron and X-ray tomography for detecting and analyzing microplastic particles in a sand column (Tötzke et al., 2021b). While neutron tomography was the key step in detecting MP as hydrogen-rich particles, the analysis of corresponding X-ray images enabled the unambiguous identification as MP particles and provided complementary 3D information about the sand matrix. Other tomography approaches for MP detection seem not yet available.

With the current work, we aimed to advance the development in two directions: Firstly, testing the potential of the method to detect microplastic particles in more natural soil environments and, secondly, detecting microplastic particles with smaller dimensions and different shapes. The sand used in the pilot study of Tötzke et al. (2021b) was just a simplistic approximation of natural soils. But now we have improved the samples to contain more of the organic components usually present in natural soils. However, being able to distinguish between microplastic particles and organic soil components represents a major challenge in natural soil samples. As a first step to better mimic natural soil conditions, we tested the detection and localization of MP particles in sand mixed with different organic components. In a further step, we then also used natural sandy soil, in some cases together with a living plant root system. Furthermore, we demonstrated the capability of detecting smaller MP with different shapes in natural sandy soil and finally discuss potential applications, challenges and limitations of this non-invasive analytic approach.

2. Material and methods

2.1. Sample preparation

A first set of samples was prepared to test the detectability of MP particles in sand enriched with organic components, mimicking a sandy soil environment. Six boron-free glass cylinders (designated as specimen group #A) with an inner diameter of 20 mm and a height of 80 mm were used to hold the sand columns containing a predefined number of MP particles. Sand (type FH 31, Quartzwerke Frechen/Germany) was mixed with various organic additives at a concentration of 2 wt%. MP fragments with a maximum edge-to-edge length of 0.5–2 mm were prepared from standard plastic materials, covering three different polymer types: polypropylene (PP), polystyrene (PS), and polyethylene terephthalate (PET). The sand columns were divided by paper disks into three distinct compartments each containing five particles of one type of plastic, as illustrated for sample #A_peat in Fig. 1a. Three natural materials served as organic additives for the sand to simulate different types of particulate organic matter present in a sandy soil environment: peat was added to samples #A_peat and #A_peat_H_2O_2, bark mulch to #A_bark and #A_bark_H_2O_2 and finally charcoal to samples #A_char and #A_char_H_2O_2. One sample from each group was treated for seven days with 30 % vol. H_2O_2 solution (indicated by index "_H_2O_2") as pre-processing method to decompose the organic matter in the sample and facilitate the identification of MP particles during the segmentation process. This treatment has been used in a similar way when processing destructed soil or sediment samples (Munz et al., 2023a), usually after separation of grains from the filtrate containing the MP. Here, however, it was applied to the intact sample.

A second set of samples was prepared to investigate the feasibility of detecting different MP particle shapes in natural soil. (i) Fragments of different polyethylene films used in asparagus cultivation were mixed with natural sandy soil collected from an asparagus cultivation field near Beelitz, Brandenburg, Germany and filled into a boron-free glass container with an inner diameter of 20 mm and a height of 80 mm. (ii) A PTFE cylinder with an inner diameter of 9 mm served as sample holder for MP fibers, which were also embedded in natural sandy soil collected from the "Chicken Creek" catchment near Cottbus, Germany (Dara et al., 2015). (iii) Finally, two samples were prepared to test the detectability of MP in soil columns containing a living root system. Lupine plants were grown in boron-free glass cylinders (27/30 mm inner/outer diameter, 100 mm height) also filled with sandy soil collected from the "Chicken Creek" catchment, mixed with either polycarbonate particles or PP film fragments at a concentration of 0.4 % wt/wt. Plants were grown in a plant growth cabinet according to the protocol described in Tötzke et al. (2017), and scanned at the neutron imaging station ten days after planting at a soil water content of 0.04 cm^3cm^{-3}.

2.2. Dual-mode neutron and X-ray tomography for detecting MP

All 3D imaging experiments were performed at the neutron and X-ray tomography station "NeXT" at the Institut Laue-Langevin (ILL) in Grenoble, France. A curved neutron guide delivers cold neutrons from the ILL's 58.3 MW high-flux reactor to the imaging station, where for performing the tomography the sample is placed in front of a neutron detector at a distance of 10 m from a group of pinholes (Tengattini et al., 2020). Using the largest pinhole with 30 mm in diameter, the neutron flux at the measuring position is high (about $3.8 \cdot 10^8$ neutrons $cm^{-2} \cdot s^{-1}$) with a L/D ratio of 333. The medium-resolution detector consists of a 50 μm thick ^{6}LiZnS:Ag scintillator screen (converting incident neutrons into visible light) and a sCMOS camera (Hamamatsu Orca 4V2) combined with a high aperture Canon photo lens (aperture f./1.2, focal length 50 mm) (Tötzke et al., 2019). After binning (2 × 2) an effective pixel size of 48.6 μm was obtained, resulting in a physical spatial resolution of 100 μm estimated from the "Siemens star" test pattern (Kozhuharova, 2022). The exposure time was set to 1 s and a total of 3 images were averaged for each angle in order to improve the statistics. 736 projections were captured over an angular range of 360° resulting in a total acquisition time of approximately 40 min per scan. To better resolve the fine structures of MP films and fibers, we used the high-resolution neutron

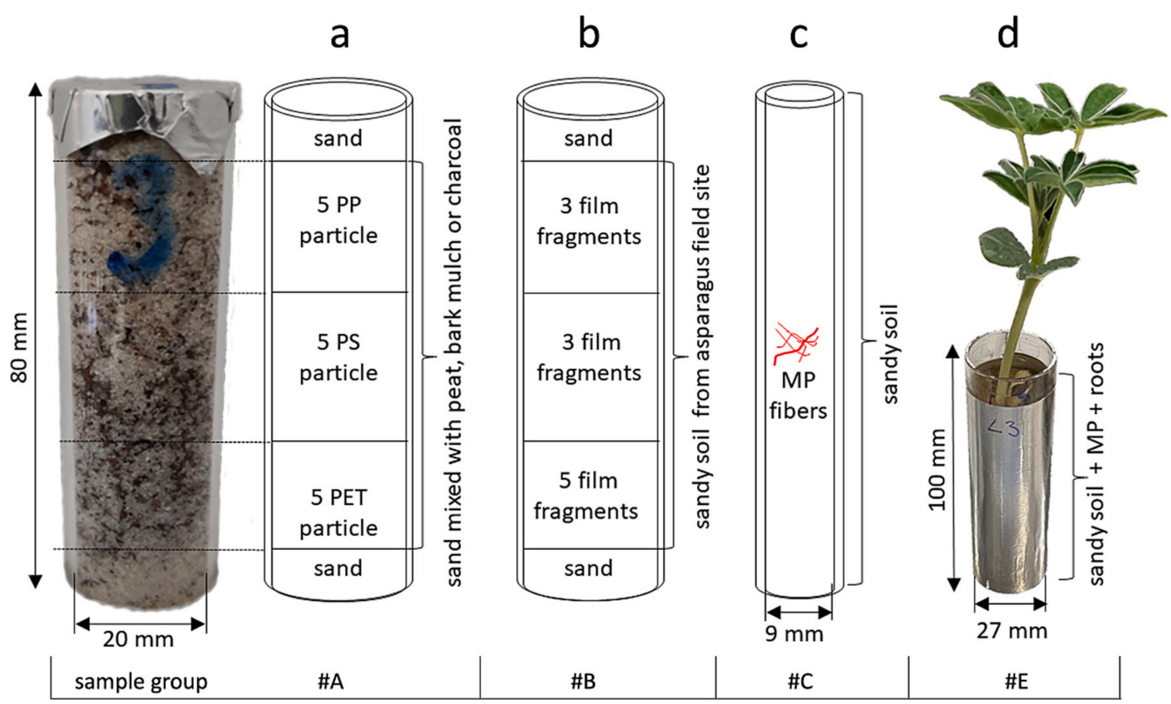

Fig. 1. Sample designs for analysis of MP particles in sandy soil environments a) Photograph and schematic drawing of vertically partitioned sample cylinders each containing different MP particles embedded in sand that was amended with one of the three natural organic materials (and one of these two was subjected to H_2O_2 treatment as a pre-processing step); b) Partitioned sample cylinder containing MP film fragments embedded in natural sandy soil; c) Sandy soil column containing MP fibers in its center; d) Lupin plant grown in sandy soil containing either polycarbonate MP particles or polypropylene film fragments.

detector with a pixel size of 16 μm, which is described in detail in Tengattini et al. (2020).

The X-ray setup included a microfocus X-ray source (type L12161–07, Hamamatsu Photonics, Hamamatsu, Japan), operated at an acceleration voltage of 100 kV and a current of 300 μA, and a flat panel detector (type PaxScan® 2530HE, Varex Imaging cooperation, Salt Lake City, USA) (Tengattini et al., 2020). The source-detector and source-object distance were set to 507.5 and 182.6 mm, respectively, resulting in an effective pixel size of 50 μm. Here also 736 projections were acquired over an angular range of 360°. Neutron and X-ray radiographs (projection images) were corrected from flatfield and darkfield images and reconstructed using a filtered back projection algorithm.

2.3. Image registration

The evaluation of bimodal tomography data sets generally requires image registration. This involves adjusting the spatial resolution and precisely aligning the data to obtain congruent three-dimensional X-ray and neutron images of the samples. Registration of bimodal data sets is particularly challenging because the gray scale and contrast levels of individual phases can vary substantially from one modality to another. We used the registration software called "spam" (Stamati et al., 2020) to register the set of samples containing MP particles in sand enriched with organic materials. The remaining samples, i.e., the soil samples containing MP film fragments, MP fibers and lupine roots, were registered using the software "Fiji". The field of view, spatial resolution, and 3D orientation of the volume datasets were manually adjusted similar to the procedure described in Haber-Pohlmeier et al. (2019).

The X-ray tomography (CT) data was used as reference during image registration with "spam", which means that the voxel size, the canvas size, and the number of tomographic slices of the neutron tomogram were adapted to the dimensions of the CT images. The multimodal registration algorithm is considered as an extension of classical digital image correlation methods (Roubin et al., 2019). Its goal is to determine the linear transformation operator F, affecting the coordinates of one modality image, in our case neutron tomography (NT), so that it matches the reference image, here X-ray CT. Prior to the actual registration in "spam" the NT data were scaled to the spatial resolution of the CT dataset and roughly aligned manually using "Fiji". For robustness and speed, "spam" prefers to register highly downscaled images, which eliminates high-frequency variations (Roubin et al., 2019). Therefore, 2 × 2 × 2 and 4 × 4 × 4 binning was applied to all 3D images for registration. After downscaling, the 4-binned NT and CT volumes were loaded into "spam" to undergo the registration step of the workflow. The first part of the registration involved a manual selection of translation, rotation, and scaling parameters for all three dimensions (x, y, z) of the NT image to be registered. This process resulted in a basic transformation matrix, which was used later on as the initial stage of a 200-step iteration mechanism to obtain a refined transformation matrix. In the second step, five different material phases were identified: air, glass container as well as larger quartz sand particles, finer quartz sand particles, organic matter with smaller neutron attenuation coefficient, and MPs and organic matter with greater neutron attenuation coefficient. The similar attenuation properties of MP (synthetic organics) and natural organic matter made the segmentation process challenging. "spam" works on the principle of a fitted joint histogram (Gaussian distribution mixture form), i.e., the phases are each characterized by a bivariate Gaussian distribution, where the bivariate refers to the two 3D measurements of their attenuation properties for neutrons and X-rays, gathered into a vector (Roubin et al., 2019). From this histogram, the five maxima were selected, and five Gaussian ellipsoids were fitted. The phase diagram was then computed using these fits with a target voxel coverage of 99 %. Finally, the linear transformation operator F was updated over the iterations, resulting in the extraction of translation, rotation, and dilation. The convergence condition was set to a value of 0.01. After convergence at the 4-binning level, the F operator was rescaled (translation part multiplied by 2) and was used as an initial guess for the 2-binning level. A repetition of registrations was performed on progressively more detailed images using the previously obtained transformation as the initial condition. The validity of the registered results was visually checked in a checkerboard pattern generated in "spam" by mixing the NT and CT, as shown in Fig. S1 in the Supplementary Information.

2.4. MP segmentation and 3D visualization

Data visualization and segmentation of MP particles were performed using the rendering software "VGSTUDIO MAX" (Volume Graphics, Heidelberg, Germany, version 3.1). In terms of 3D image processing, the program allows versatile user interaction directly at the level of the reconstructed 3D sample volume. A 3D rendered view of the reconstructed sample volume is generated by setting various rendering parameters, such as gray-scale value thresholds and opacity curves in the 3D histogram. This proved to be very beneficial when using the implemented region-growing algorithm for segmentation, which is initiated by manually positioning the growth seeds. To enable reliable subjective identification of MPs, a 3D view was generated showing only the components with the strongest neutron attenuation (c.f. Fig. 2B). Due to their similar neutron attenuation properties, it is not possible to clearly distinguish between MP and natural soil organic particles just using global thresholding alone. However, the potential MP particles could be selected based on their specific angular shape by optical inspection in the 3D view to place the seeds for the actual segmentation algorithm. At these points, a region of interest (ROI) was created for each MP particle at these seed points and then extended to neighboring voxels if they were similar enough, i.e., if the deviation of the gray level values did not exceed a predefined threshold. After the initial segmentation of the MP particles in the NT image, their shape and size were verified by copying the corresponding ROIs onto the CT image volume and manually checking each particle using the CT images as a point of reference. The main criterion was whether the edges of the MP particles were placed in a way so that they did not overlap the edges of neither the mineral particles nor the organic material. In summary, the segmentation procedure involved global thresholding to render a 3D neutron image of the most attenuating sample components, a subsequent subjective particle selection using prior knowledge of the number, specific size, and shape of MP particles and finally a validity check of the size and shape of the segmented region in the complementary X-ray image.

3. Results

3.1. Detecting different microplastic particles in sandy environment containing peat

First, we present exemplary results for sample #A_peat containing sand-peat mixture without H_2O_2-treatment. Fig. 2 shows an image series of the reconstructed neutron tomogram, rendered with an increasing gray-scale level threshold to visualize the individual components. The sample had been divided in 5 vertical sections by four paper separator disks (Fig. 2a). The three central compartments each contained five MP particles made of PP, PS or PET (from top to bottom) embedded in a sand-peat mixture (2 % by weight).

While the bottom and top of the sample (filled with pure sand) appear almost transparent in Fig. 2b, the attenuation of neutrons by the peat added severely limits the visibility of the microplastic particles in the central compartments. By increasing the gray level threshold, the peat material was progressively faded out, revealing the three groups of MP particles (Fig. 2C-F). The mean local neutron coefficients measured in the core region of the particles differ significantly: $\mu_{neutron} = 1.7\ cm^{-1}$ for PET particles, $3.0\ cm^{-1}$ for PS, and $4.7\ cm^{-1}$ for PP particles. This is mainly due to the different elemental hydrogen content in the molecular structure of the plastics (PET: $C_{10}H_8O_4$, PS: C_8H_8, PP: C_3H_6). For PET

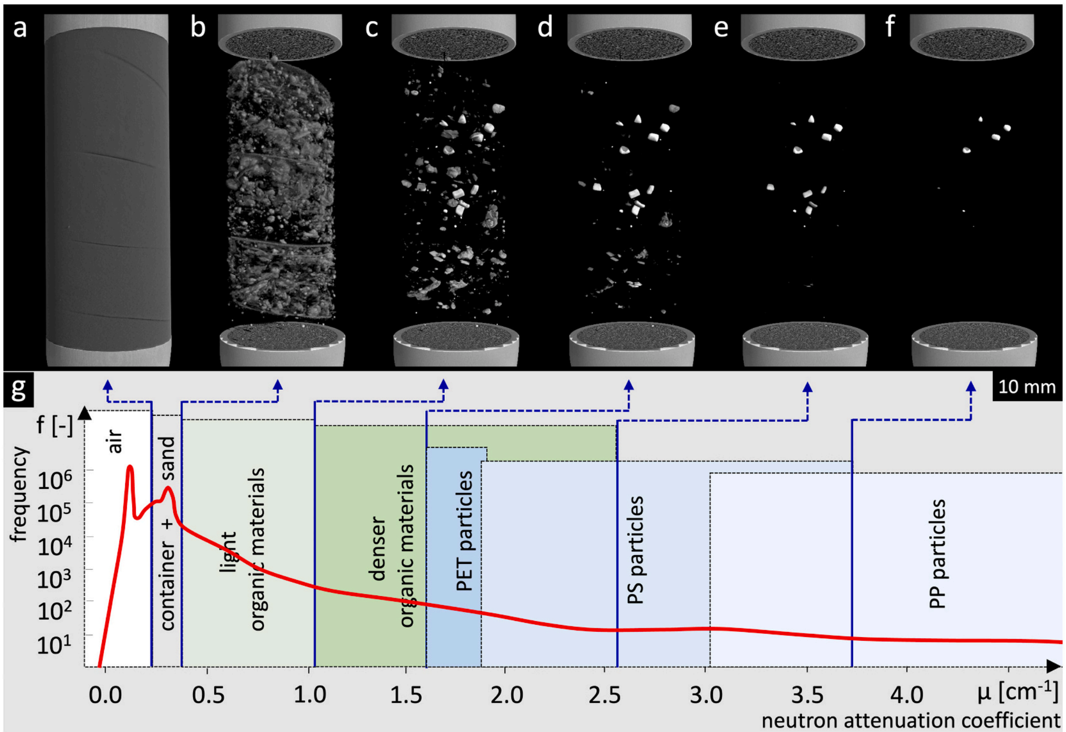

Fig. 2. Tomography of a sample containing three groups of MP particles embedded in a sand column amended with peat. Shown are the steps to visualize particles with different attenuation levels. a-f) The 3D neutron data were rendered using an increasing gray-scale threshold to reveal the individual components of the sample. Note that the top and bottom of the sample are rendered from the X-ray tomogram to facilitate spatial visualization of the sample. g) Histogram of the 3D neutron image. The thresholds used for 3D rendering are shown as vertical blue lines, and the range of measured local neutron attenuation coefficients is indicated for the major material phases. The range of attenuation coefficients of PET particles is in the range of the denser peat material, which makes segmentation of these particles difficult.

particles, the small size and flat shape may also contribute to the lower value of the measured attenuation coefficient due to the limited image resolution, as the apparent attenuation coefficient decreases towards the edges of the particles (partial volume effect). The resulting ranges of $\mu_{neutron}$ for the corresponding material phases are shown in Fig. 2G. Peat consists mainly of partially decomposed vegetation and other organic material. When mixed with the sand, loosely packed fibrous peat material is partially separated and dispersed from more compact plant debris, resulting in strong local density variations and thus variations in local attenuation coefficients within the central sample compartments. This is not critical for the extraction of PS and PP particles as they have substantially higher neutron attenuation coefficients, allowing image segmentation by global thresholding. However, the very similar attenuation properties of the denser peat fraction and PET particles (see Fig. 2G) make the segmentation of these particles challenging (see also Movie S1 in SI). Fig. S2 shows the cross-section of a PET particle and a peat agglomerate as a neutron (Fig. S2 b) and X-ray (Fig. S2 c) tomography section. Both PET and the peat material behave similarly in terms of attenuation, i.e., strong attenuation of neutrons and low attenuation of X-rays. The difference in local X-ray attenuation coefficients (mainly due to different material densities) here is too small to allow a simple and clear distinction between MP and organic soil material.

In addition to microplastics and soil organic matter, there are some other particles in the sample that are characterized by very high neutron attenuation (Fig. S3b). These particles are most likely organo-mineral in nature and can be clearly distinguished from the MP and pure organic components in the X-ray image (Fig. S3c), as already described by Tötzke et al. (2021b).

Since the differences in attenuation behavior between MP particles and peat are not very pronounced, the shape and size of the MP particles were introduced as an additional distinguishing criterion. Upon close visual inspection of the 3D rendered neutron data, all MP particles could be clearly identified by their specific angular shape and virtually extracted using the region growing algorithm implemented in "VGStudioMax" (see Supplementary Information Fig. S4). A magnified view of the virtual extracted MP particles is shown in Fig. S4c-S4e and compared with the original photograph of the MP particles placed in the sample. The good agreement between the 3D shapes extracted from the tomography and 2D views obtained with the light microscope demonstrates the great ability of this method to reproduce the shape and size of MP particles in three dimensions and confirms that the spatial resolution was chosen reasonably with respect to the size of the MP particles to be detected.

3.2. Detecting microplastic particles in sandy environment containing different organic additives and using H_2O_2 treatment

The next step was to qualitatively evaluate how the addition of different organic materials, namely peat, bark mulch and charcoal, affected the detectability of MP particles in the sand. In addition, it was tested to what extent the interference of the MP detection by the organic matter in the soil could be reduced by the treatment of the samples with H_2O_2. Fig. 3 provides an overview of the complete set of sample group #A, with the above-mentioned organic amendments with and without H_2O_2-treatment. After applying a global threshold, the number, shape and size of non-plastic particles still visible in the neutron image strongly depend on the type of organic material added (Fig. 3a, c and e). The most and largest non-plastic particles were detected in sample #A_bark. Non-plastic particles were also found in large numbers in sample #A_peat, but their average size was substantially smaller. The fewest non-plastic particles were found in sample #A_char. The comparison between treated and untreated samples (Fig. 3a vs. b, Fig. 3c vs. d, and Fig. 3e vs. f) clearly shows that a prior sample treatment with hydrogen peroxide solution facilitates the detection of MP particles as

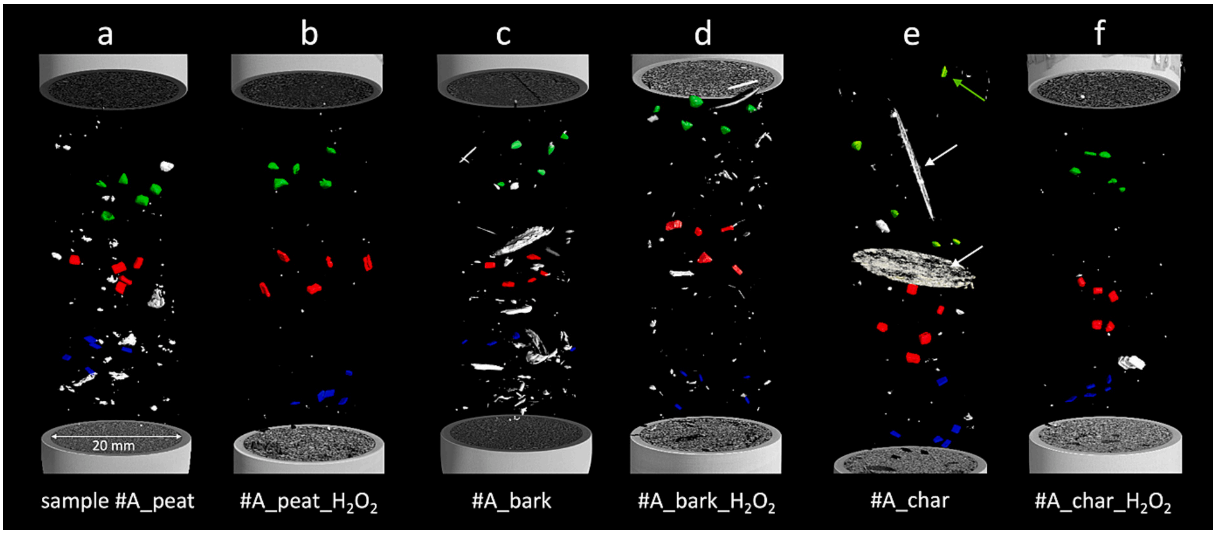

Fig. 3. MP particles in sand with different organic additives: a + b) peat; c + d) bark mulch; e + f) charcoal. The central part of the samples shows the components with the highest neutron attenuation: PP particles are colored in green, PS particles in red, PET particles in blue, and non-plastics in white-gray. The top and bottom parts of the sample are shown as a 3D rendered X-ray image to facilitate spatial orientation. Samples with name index "_H_2O_2" were treated with H_2O_2 prior to imaging. Note that sample #A_char was accidentally tilted during preparation, causing the upper separator to shift and a PP particle to escape from the upper compartment. Two paper separator disks and the displaced PP particle are marked with white and green arrows.

fewer strongly attenuating, non-plastic particles were detected for all three organic additives.

3.3. Using shape descriptors to improve the detection of microplastic particles in sandy environment containing organic additives

The segmentation of MP particles by region-growing algorithms is based on subjective classification of MP particles according to their specific shape characteristics. Alternatively, objective shape criteria can

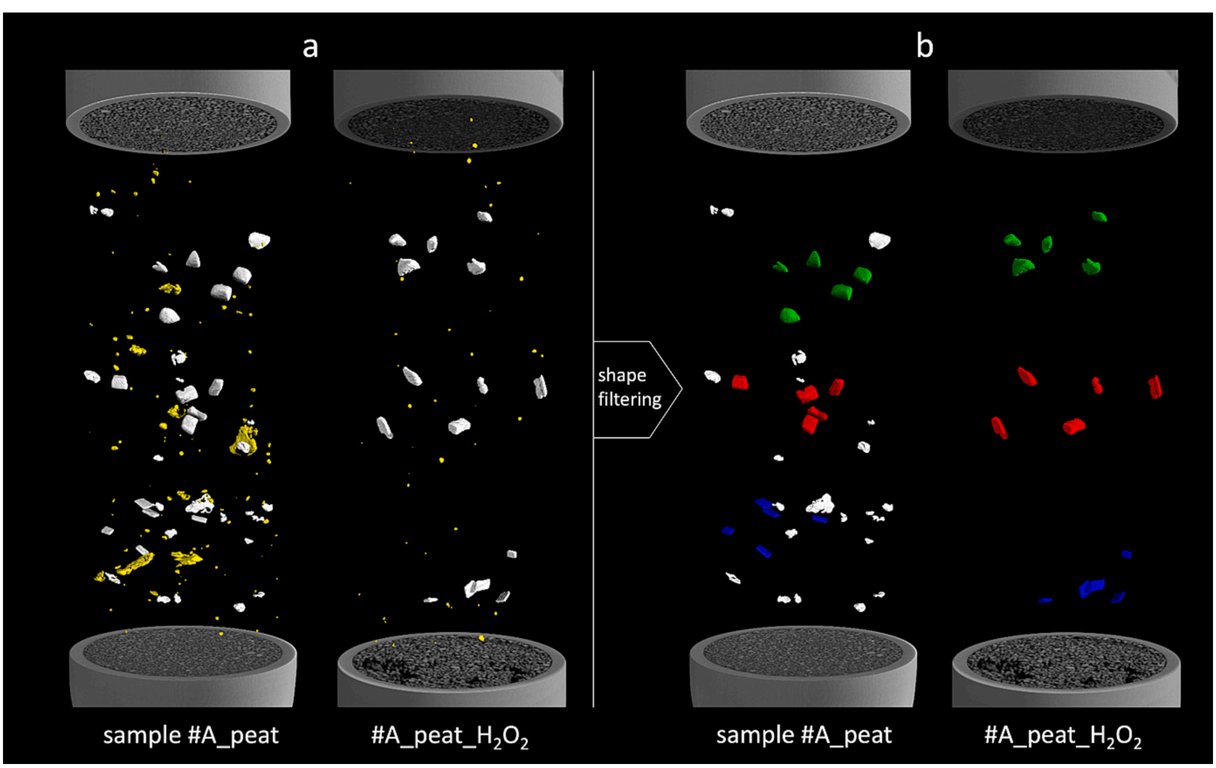

Fig. 4. Testing the objective classification of MP particles using simple shape filter criteria. a) Samples #A_peat and #A_peat_H_2O_2 containing peat, the latter treated with H_2O_2. After global thresholding, sphericity index, surface area, and Euler number were calculated for all particles. Particles displayed in yellow were outside the range defined for individual shape descriptors of MP, and consequently sorted out. b) Result of the shape filtering: the colored particles are the true microplastic particles, the white particles are the remaining misclassified peat particles (left tomogram, #A_peat). Note that no misclassified particles remain for the H_2O_2 pre-treated sample (right tomogram, #A_peat_H_2O_2).

be used to extract the MP particles from the set remaining after grayscale level thresholding. We tested a simple approach that computes several shape descriptors, namely the sphericity index, the surface area, and the Euler number. Since the microplastic particles encountered in this study have characteristic shape and size spectra, ranges could be defined for each shape descriptor. In this way, particles outside these ranges could be filtered out. Fig. 3 illustrates this procedure for samples #A_peat and #A_peat_H_2O_2, both containing peat, but the latter having been treated with H_2O_2 solution. Fig. 3a on its left shows the highly attenuating particles of sample #A_peat after adjusting the grayscale level threshold. Yellow rendered particles were outside the range of at least one of the shape descriptors and were consequently discarded as non-plastics. The particles remaining after shape filtering are shown in Fig. 4b on its left. The particles rendered in white are misclassified, i.e., non-plastics that could not be sorted out by the shape filtering. Fig. 4a shows on the right the highly attenuating particles of sample #A_peat_H_2O_2 after grayscale level thresholding. Due to the H_2O_2 treatment, there are significantly fewer non-plastic particles, and they are also significantly smaller. Finally, when shape filtering was applied to the H_2O_2 treated sample, detection was more successful, and all MP particles were found with not a single misclassified particles remaining (Fig. 4b, on the right).

3.4. Detection of microplastic films and fibers in sandy soil

The second part of this work tested the ability of the method to detect smaller microplastic particles, in particular plastic film fragments and fibers, through the preparation of samples of practical relevance. One set-up was mimicking MP in an asparagus field soil in the region. Using the medium-resolution neutron setup with an effective pixel size of 49 μm and a corresponding physical spatial resolution of 100 μm, the entire soil sample could be captured in one go (Fig. 5a). The semi-transparent 3D neutron image shows the three soil compartments, each containing a group of PE film fragments. With a thickness of 50 μm the size of the film fragments was slightly below the resolution limit of the setup. However, they are still clearly visible in the image due to the favorable contrast between the highly-neutron attenuating PE material and its dry soil environment. In order to capture more details, the upper part of the sample was additionally imaged with a special high-resolution neutron detector in a reduced field of view (Fig. 5b, pixel size 16 μm). The film fragments are visible as continuous structures, and their shape and orientation can be identified well. The combination with the registered 3D X-ray image (Fig. 5c and d) allows further consideration of how the PE film fragments are embedded in the soil matrix and also that the microstructure of the soil matrix is disturbed by them, affecting its properties.

Using the same high-resolution neutron detector system in combination with the X-ray scanner, we tested the potential of the method to detect the shape, position, and orientation of flat-shaped MP fibers embedded in a 9 mm diameter sandy soil column (Fig. 1c). The plastic fibers were arranged in a group at middle height of the soil column (Fig. 6). After wetting and subsequent drying of the sample, a crack had developed in the soil matrix along the fiber plane, indicating a planar weakness in the soil matrix structure introduced by the fibers. This crack is clearly visible in the X-ray image, but the microplastic fiber inside causing the crack is barely detectable, if at all (Fig. 6a). Thus, because of the low contrast between the plastic and the air-filled pore space, X-ray tomography can primarily, and perhaps only, identify the void in the soil matrix. Neutron tomography, on the other hand, can clearly identify MP even in the apparently open void (Fig. 6b, bright structure). The implication is that the neutron tomography alone, at least much better, is able to recognize that the crack at this position is not an empty crack but contains the solid material of a microplastic fiber, that even

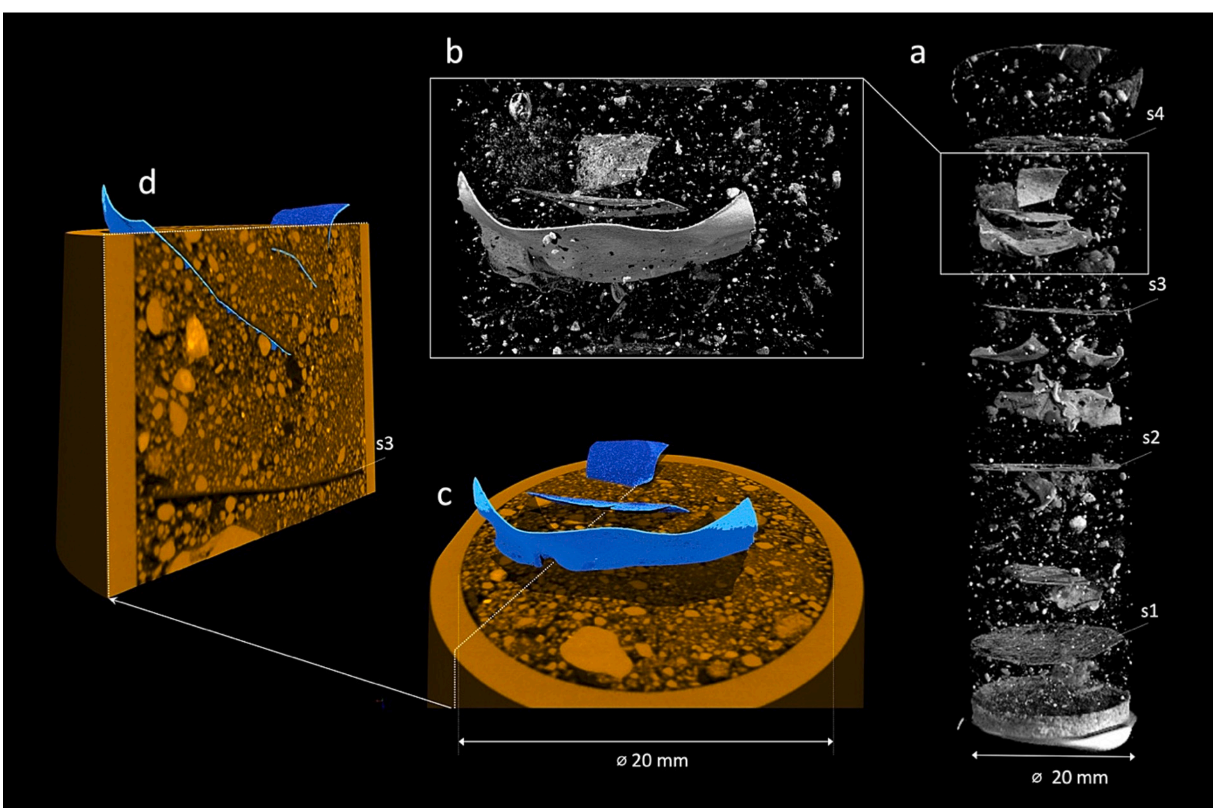

Fig. 5. Sample #B containing fragments of polyethylene film used for asparagus cultivation in natural sandy soil. a) Half-transparent neutron image (49 μm/pix) of the soil sample showing three groups of MP film fragments separated by the four cardboard disks (labeled as s1 - s4). b) Higher resolution tomogram (16 μm/pix) of the upper compartment. c + d) The three film fragments (blue) present in this compartment were extracted from the neutron image and rendered together with the registered X-ray data. The virtual cross sections show how the plastic film fragments are embedded in the soil matrix.

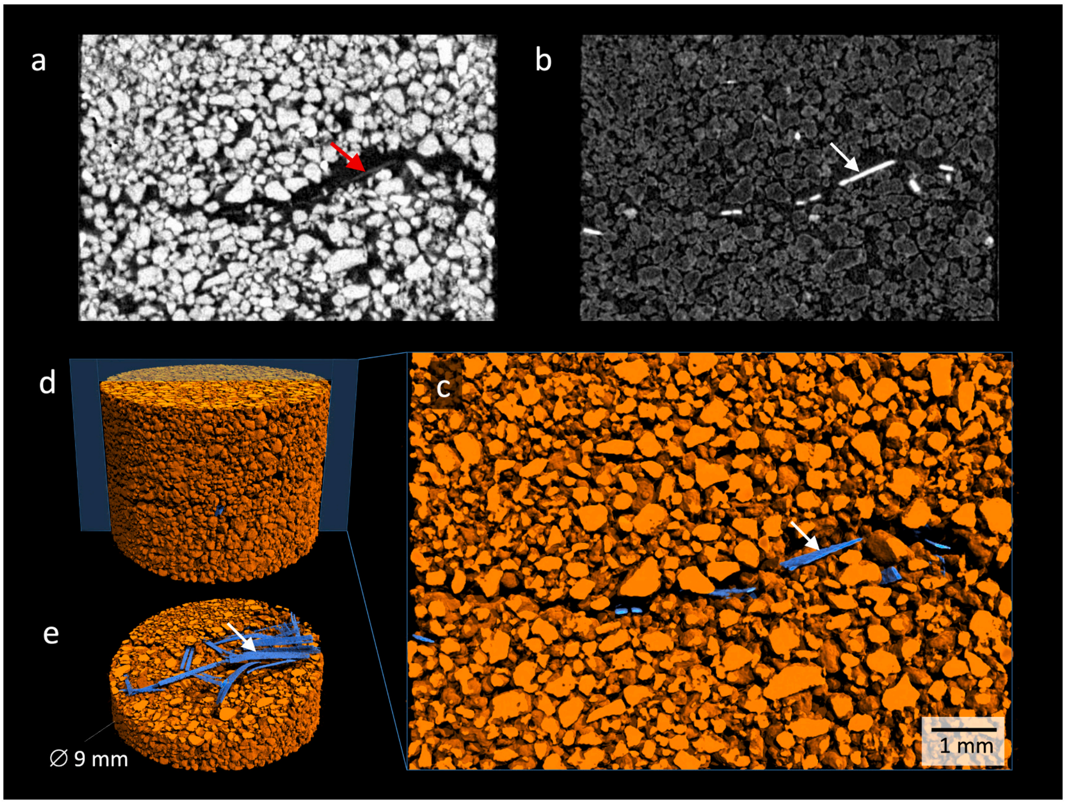

Fig. 6. Dual-mode tomography of sample #C, flat-shaped microplastic fibers embedded in a natural sandy soil. White and red arrows indicate the same position pointing to a plastic fiber. a) Vertical 2D cross section of the X-ray tomogram; b) Vertical 2D cross section of the neutron tomogram; c) Vertical section of the combined tomogram (X-ray +neutron): the fibers induced a crack in the soil matrix; d) 3D rendered image of the soil column; e) Virtual horizontal section of combined tomogram unveiling the embedded microplastic fibers (rendered in blue, thickness ~ 50 μm).

contributed to the formation of the crack. This insight will make a big difference in the interpretation of the crack evolution, but also in the consequences, e.g., in terms of water flow and mechanical stability. The combination of the tomography approaches (Fig. 6c) provides a complete picture of the soil matrix, the crack and the microplastic fibers within it. The crack ran through the entire cross-section of the soil column, as can be seen in Fig. 6a and the video sequence provided in the Supplementary Information (Movie *S2*). Thanks to the complementary nature of the X-ray and neutron imaging modalities, the 3D arrangement of microplastic fibers within the soil matrix can be completely identified (Fig. 6b).

3.5. Detection of microplastic particles in root-soil systems

Finally, we tested the detection of differently shaped microplastic particles, specifically polycarbonate fragments and PP film fragments, in root soil systems. For this purpose, ten-day-old lupine plants grown in a mixture of sandy soil and MP particles were imaged at the low soil moisture level (0.04 cm^3 cm^{-3}), which allowed good contrast between MP and soil and between roots and soil. A particular challenge in segmenting this neutron image data is distinguishing the root structures from the MP, since the root tissue and the plastic material have similar attenuation properties (Fig. 7a, for the polycarbonate MP). First, the roots were segmented in the neutron image (Fig. 7b). The root system has a clearly defined tap root and a large number of lateral roots, some of which have started to grow along the container walls. At several locations the lateral roots have developed cluster roots bundles, which have been shown by imaging studies to be hotspots of water uptake (Dara et al., 2015) and respiration activity (Bereswill et al., 2021), which may also have implications for translocation of smaller MP particles. Then the potential MP particles were segmented in the neutron image again by region growing (Fig. 7c&d).

In the next step, the X-ray data were registered to integrate the complementary information about the microstructure of the bulk soil into the neutron image (Fig. 7e&f) and to verify the detection of microplastics by neutrons. For the latter, the corresponding regions of interest in the X-ray image were analyzed. Only voxels with low X-ray attenuation were confirmed to belong to the microplastic fraction; the voxels with higher attenuation (gray-scale value) were identified as organo-mineral particles and thus discarded (Fig. 7g +7 h). While the majority of the potential MP particles identified by neutron tomography could be confirmed as true microplastic particles by X-ray attenuation, a significant number had to be discarded because their X-ray attenuation characteristics did not match MP characteristics. Therefore, the dual tomography approach was required to identify the polycarbonate fragments, but ultimately these microplastic particles could be identified as well as the root system. The microplastic particles showed no obvious spatial correlation to the root system, except that some MP fragments must have been pushed aside by the growing tap root. However, it cannot be excluded that the presence of the microplastics locally influenced the formation of the root system, especially in the case of lateral roots, including cluster roots.

A semi-transparent 3D representation of the lupine root sample grown in a mixture of sandy soil and polypropylene film fragments is shown in Fig. 8a. The segmentation of the root structure and the MP film fragments (Fig. 8b&c) was performed according to the procedure described above. The distinctly flat shape of the MP film fragments still seemed to allow for complete localization of the individual MP particles. And this specific shape even made their identification in the neutron image more reliable. This was reflected in the subsequent validation step using the X-ray data, where not a single false detect was found (Fig. 8d). Thus, for these types of film fragments a neutron tomography alone

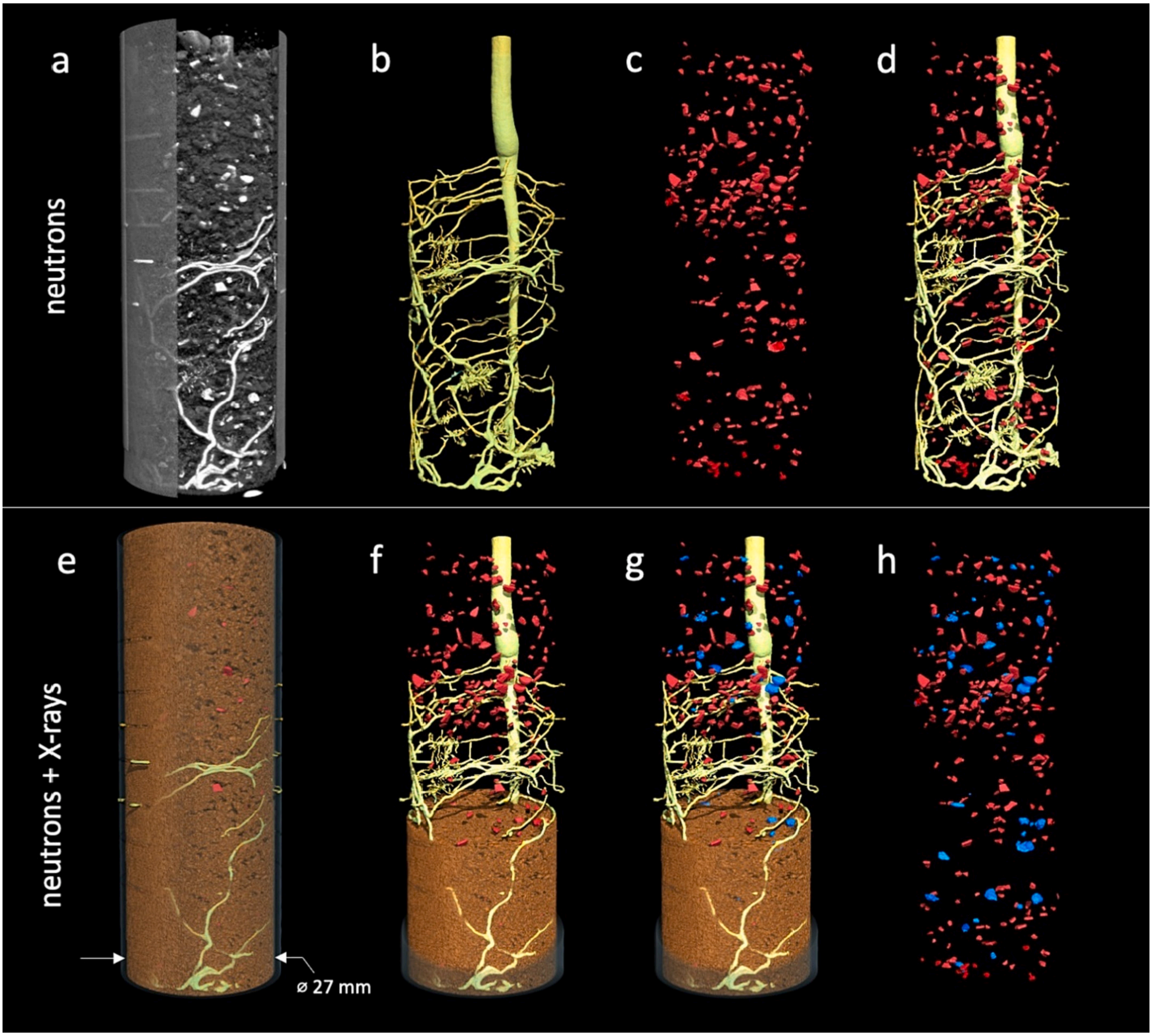

Fig. 7. Dual-mode tomography of a lupin root system grown in sandy soil containing polycarbonate fragments (sample #D1). a) 3D rendered image of the reconstructed neutron tomogram; inner ø of the container is 27 mm, voxel size is 35 μm; b) Segmented root system with emerging cluster roots; c) Distribution of microplastics as detected by neutrons; d) Root system + microplastics; e) Registered X-ray tomogram augmented with the complementary information shown in (d); f) Virtual section of container and soil revealing roots and microplastics; g + h) Appropriate thresholding of the histogram of the X-ray tomogram verifies plastic detection by neutrons and allows deselection of erroneously detected particles (marked in blue), as outlined in Tötzke et al. (2021b).

could be sufficient for identifying roots and MP in soil.

4. Discussion

The addition of hydrogen-rich organic material poses a challenge for MP identification, as it makes the sample structure more complex and increases the background signal. In addition, the detectability of microplastics is dependent on both the type of polymer and the size of the particles. The larger the particle and the higher its elemental hydrogen content, the easier it was to identify in the 3D neutron images. The overlap of the denser organic material with the PET particles in the histogram (Fig. 2g) indicates that these material phases cannot be clearly distinguished from each other based on neutron attenuation characteristics alone. In contrast to organo-mineral particles with high neutron attenuation, which could be clearly distinguished from microplastics in the complementary X-ray image, plant materials such as peat or bark mulch show similarly low X-ray attenuation as MP (c.f. Fig. S2 and S3). This means that the simple bimodal thresholding, as performed by Tötzke et al. (2021b) for the case of pure sand, is not sufficient for natural soils with non-negligible organic carbon content. Segmentation requires a more sophisticated approach that considers complementary image features such as shape, gradients, edges, or texture. In our case, all the MP particles could be identified by their specific shape in the neutron image and segmented using a region growing algorithm (Fig. S4). The sand matrix accessible from the complementary X-ray image was used as a 3D reference structure to validate the position of the particle edges and thus accurately determine the shape and size of the MP. This is true for all samples, whether they had been treated with hydrogen peroxide or not. The addition of various organic materials interfered with the detection of MP particles to

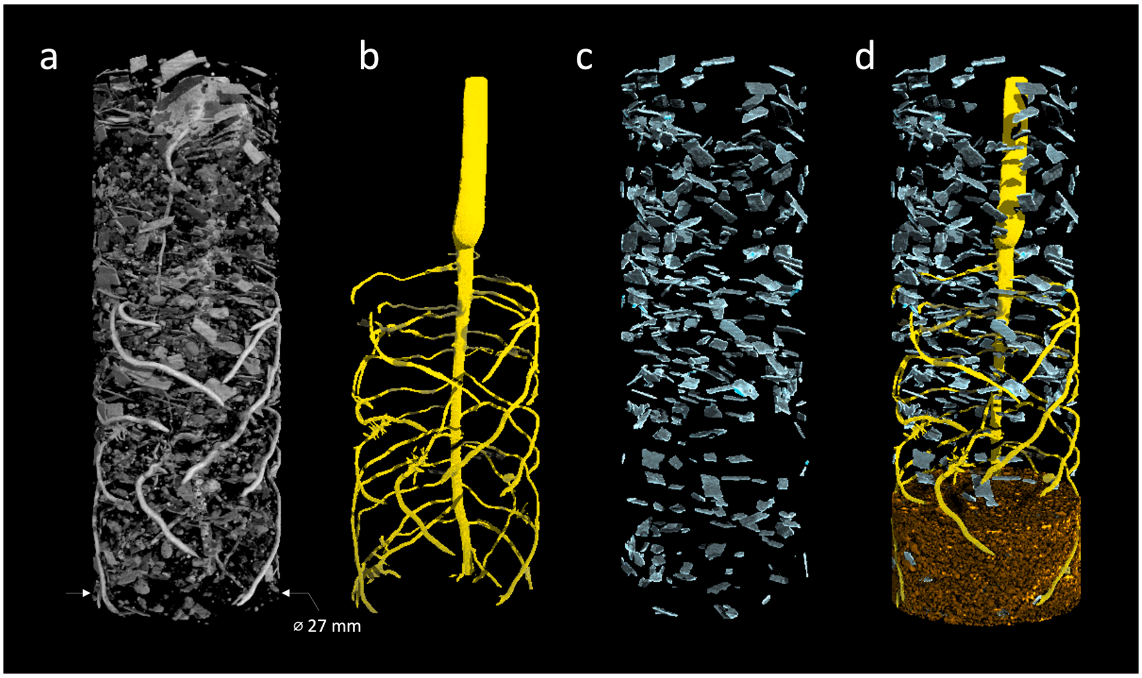

Fig. 8. Dual-mode tomography of a lupin root system grown in sandy soil containing fragments of a polypropylene film (sample #D2). The opaque visualization of the thin film fragments is needed to make them clearly visible, but may give a false impression of a seemingly high MP volume content in the sample; a) 3D rendered image of the reconstructed neutron tomogram; b) Segmented root system with emerging cluster roots; c) PP film fragments segmented from the neutron image; d) Compilation of root system and PP film fragments segmented from the neutron image + registered image data of the soil section retrieved from the X-ray tomogram.

varying degrees. The variance in the number, shape and size of non-plastic particles in the neutron image (Fig. 3a, c and e) is due to the different consistency and chemical composition of the organic materials. For example, bark mulch consists of compact fragments, some relatively large, while peat has a looser, crumblier structure. Since charcoal loses most of its volatile hydrogen compounds during pyrolysis, it is the organic material with the lowest neutron attenuation. Treatment with hydrogen peroxide solution facilitated substantially the detection of MP particles because a significant fraction of the soil organic matter had been digested by the reactive H_2O_2 solution. The differences observed between the samples (Fig. 3b, d and f) reflect the different reactivity of the organic amendments. While peat was apparently almost completely digested due to its high specific surface area and high chemical reactivity, the comparatively compact and chemically more inert bark mulch pieces were only partially digested. The better the chemical degradation, the fewer highly attenuating, non-plastic particles remained in the sample, which in turn meant that fewer non-plastic particles needed to be distinguished from the MP particles. However, since hydrogen peroxide solution treatment can also affect the microstructure of the sample, it should only be considered as a last resort, depending on the scope of the study, when image segmentation of untreated samples fails due to the high organic content of the soil.

MP detection via the region growing method, as used in this study, works by subjectively recognizing the specific particle shape in the neutron image and then manually positioning the growth seed. This method worked so well in this case because it exploited the human eye's strong shape recognition capabilities for subjective classification, and the number and shape of MP particles were known from sample preparation. This qualifies the method especially for laboratory experiments where specific properties of MP are known and MP concentrations move in predefined orders of magnitude. However, in cases where soil samples contain a large amount of MP particles, manual selection can easily become time consuming and therefore inefficient. Alternatively, simple shape descriptors such as sphericity, Euler number or specific surface area of the MP particles could be considered to generate filter criteria for an objective selection processed in an automated procedure. We have clearly demonstrated that by combining these simple criteria, it is possible to identify most MP particles. However, when using only these three simple criteria the detection can still be subject to errors and the number of false detections will increase with increasing similarity between organic particles and MP particles. Identification becomes particularly difficult when MP particles might be surrounded by organic matter, as the image contrast between them is low. As a result, the affected MP particles and organic agglomerates can easily be misinterpreted as contiguous regions. However, the rapid development of AI-based image segmentation algorithms suggests that dual-mode tomography will soon have the capability to reliably detect MP particles in complex structured soil samples and to analyze their interaction with the soil matrix in detail.

The second part of the study demonstrated the suitability of the method for analyzing MP in natural sandy soils. The inclusion of small-sized MP, i.e. pieces of mulch film and MP fibers further increased the detection challenge as well as the presence of a root system. Remarkably, the good image contrast and easily discernible planar shape allowed detection of the mulch film fragments in Sample #B even though the film thickness (50 μm) was well below the effective spatial resolution (100 μm) of the neutron detector (Fig. 5). By using a high-resolution neutron detector, the 3D orientation of the plastic film fragments could be visualized in more detail. The blending of the neutron and X-ray tomograms provides a clear picture of how the MP films introduce structural perturbations and barriers into the soil matrix that will affect water flow and several other properties of the soil when containing such MP film fragments (Fig. 5 c-d). Bimodal tomographic time series of the sample at different soil moisture levels are no longer limited by neutron tomography acquisition times (Tötzke et al., 2019; Tötzke et al., 2017) and could provide new insights into MP-induced effects on soil hydraulics, such as increased evapotranspiration rates, the formation of preferential water pathways, or altered soil wetting behavior. Clogging macropores or blocking effective water pathways with film fragments could significantly affect water transfer in the soil, resulting in uneven water distribution. Hot spots with high MP concentrations can make soil areas hydrophobic. This can cause these areas to be bypassed by water flows and soil moisture to remain permanently low (Cramer et al., 2023). High-speed neutron tomography could be used to directly analyze the dynamic 3D water imbibition patterns of such soil samples (Tötzke et al., 2021a; Tötzke et al., 2017).

Detecting microplastic fibers in sandy soils is even more difficult than finding film fragments. Given their quasi-one-dimensional shape it was hypothesized that the more the shape of microplastics differs from particles or structures that occur naturally in soil, the greater their potential impact on soil properties (Rillig et al., 2019). Due to their small diameter of a few tens of micrometers, the detection of microplastic fibers poses a particular challenge to the resolving power of the method. Using a high-resolution neutron setup, we were able to detect and visualize 50 μm flat microplastic fibers deposited in a layer of sandy soil (Fig. 6). The continuous crack in the soil that developed in the fiber deposition plane after repeated wetting and drying of the soil indicated that the fibers had introduced a fracture plane into the soil matrix. The example impressively illustrates the ability of the method to detect small MPs and to reveal MP-induced changes in the microstructure of the soil matrix. The minimum size of plastic fibers that can be detected by the method depends on the soil structure, which mediates the image contrast, and the resolving power of the neutron detector. Under reasonable contrast conditions, i.e. dry soil with low organic content, very thin plastic fibers less than 20 μm in diameter could be detected with a dedicated high-resolution neutron imaging setup (Tengattini et al., 2020), but in this case imaging will be challenging and require long scan times.

We have shown that by combining XCT and NT analysis different properties of the sample can be extracted. The method is, however, not suitable as a high-throughput method for serial analysis of natural soil samples, but rather as an analytical tool for laboratory experiments where soil samples are specifically analyzed for microplastics, and possibly for studying a limited number of cores from natural soils or coarse sediments. We think, however, that due to the high neutron attenuation of clay and loamy soils, the application of neutron imaging is inherently limited to sandy soils.

5. Conclusions

The dual-mode tomography method is suitable for investigating the presence of MP in undisturbed soil samples and thus also the influence of MP particles on soil properties. This non-invasive analysis makes it possible to detect the structural changes in the soil matrix and provides a basis for correlating them, for example, with changes in the soil hydraulic properties. One of the major challenges for the analysis, especially for image segmentation, is the structural complexity of natural soil samples and the similarity between natural soil organic matter and its synthetic counterpart created by microplastics.

Soils containing MP make X-ray CT less applicable as stand-alone method, as MP may not be detected as part of the solid components in the soil and, in particular, MP fibers may appear to be just voids of open cracks, leading to misinterpretations and erroneous conclusions. In contrast, stand-alone neutron tomography is prone to over-identification of potential microplastic particles (false positives). However in some situations (pre-treatment to reduce organic material in the sample or microplastics with shapes dissimilar to the constituents of the soil matrix) neutron tomography may be sufficient. In any case, the combination of the two into a dual-mode tomography is the most reliable tomography approach and has the potential to accurately detect the number of microplastic particles (larger than about its resolution), their volumes, shapes, orientation and spatial arrangement relative to other MP particles as well as to the soil matrix, though not their plastic type.

The method also opens up valuable new opportunities to investigate the influence of microplastics on the root space of plants. Our results demonstrate that we can detect microplastic particles in the spatial context of plant-soil interactions, which allows us to ask questions about the role of microplastics in rhizosphere processes, including soil aggregation. Providing access to spatially resolved information on MP distribution, microstructure and hydraulics of the local soil environment and root system architecture, tomographic studies such as the dual mode tomography (NT and CT) could be the key to a better mechanistic understanding of how MP-induced changes in soil properties affect plant performance.

Additional data, including animated image sequences, related to this article can be found online at https://doi.org/10.1016/j.scitotenv.2023.167927.

CRediT authorship contribution statement

Christian Tötzke: Conceptualization, Methodology, Investigation, Validation, Visualization, Writing – original draft, Funding acquisition. **Boyana Kozhuharova:** Methodology, Investigation, Writing – review & editing. **Nikolay Kardjilov:** Conceptualization, Methodology, Investigation, Writing – review & editing. **Nicolas Lenoir:** Methodology, Investigation. **Ingo Manke:** Writing – review & editing, Supervision. **Sascha E. Oswald:** Conceptualization, Methodology, Writing – review & editing, Supervision.

Declaration of competing interest

The authors declare that they have no known competing financial interests or personal relationships that could have appeared to influence the work reported in this paper.

Data availability

The datasets generated during the current study are accessible via the data depository of the ILL under DOI:10.5291/ILL-Data.UGA-114 or available from the corresponding author on reasonable request.

Acknowledgement

We gratefully acknowledge funding of the research presented here by the German Research Foundation (DFG project numbers 396368046 and 516672636).

References

Bereswill, S., Rudolph-Mohr, N., Oswald, S.E., 2021. Imaging rhizosphere CO_2 and O_2 concentration to localize respiration hotspots linked to root type and soil moisture dynamics. Rhizosphere (in review). preprint at doi:10.21203/rs.3.rs-1145795/v1.

Bläsing, M., Amelung, W., 2018. Plastics in soil: analytical methods and possible sources. Sci. Total Environ. 612, 422–435. https://doi.org/10.1016/j.scitotenv.2017.08.086.

Cramer, A., Schmidtmann, J., Benard, P., Kaestner, A., Engelhardt, M., Peiffer, S., et al., 2023. Ferrihydrite coating reduces microplastic induced soil water repellency. Environ. Sci.: Processes Impacts. https://doi.org/10.1039/D3EM00077J.

Dara, A., Moradi, B.A., Vontobel, P., Oswald, S.E., 2015. Mapping compensating root water uptake in heterogeneous soil conditions via neutron radiography. Plant and Soil 397, 273–287. https://doi.org/10.1007/s11104-015-2613-3.

de Souza Machado, A.A., Lau, C.W., Till, J., Kloas, W., Lehmann, A., Becker, R., et al., 2018. Impacts of microplastics on the soil biophysical environment. Environ. Sci. Technol. 52, 9656–9665. https://doi.org/10.1021/acs.est.8b02212.

de Souza Machado, A.A., Lau, C.W., Kloas, W., Bergmann, J., Bachelier, J.B., Faltin, E., et al., 2019. Microplastics can change soil properties and affect plant performance. Environ. Sci. Technol. 53, 6044–6052. https://doi.org/10.1021/acs.est.9b01339.

Guo, Z., Li, P., Yang, X., Wang, Z., Lu, B., Chen, W., et al., 2022. Soil texture is an important factor determining how microplastics affect soil hydraulic characteristics. Environ. Int. 165, 107293 https://doi.org/10.1016/j.envint.2022.107293.

Haber-Pohlmeier, S., Tötzke, C., Lehmann, E., Kardjilov, N., Pohlmeier, A., Oswald, S.E., 2019. Combination of magnetic resonance imaging and neutron computed tomography for three-dimensional rhizosphere imaging. Vadose Zone J. 18, 180166 https://doi.org/10.2136/vzj2018.09.0166.

Huang, Y., Liu, Q., Jia, W., Yan, C., Wang, J., 2020. Agricultural plastic mulching as a source of microplastics in the terrestrial environment. Environ. Pollut. 260, 114096 https://doi.org/10.1016/j.envpol.2020.114096.

Huerta Lwanga, E., Gertsen, H., Gooren, H., Peters, P., Salánki, T., van der Ploeg, M., et al., 2017. Incorporation of microplastics from litter into burrows of Lumbricus terrestris. Environ. Pollut. 220, 523–531. https://doi.org/10.1016/j.envpol.2016.09.096.

Kozhuharova, B., 2022. Non-invasive analysis of microplastic particles in soil by means of complementary 3D neutron and X-ray imaging. Institute of Environmental Science and Geography. Master Thesis. University of Potsdam.

Krehl, A., Schöllkopf, U., Májeková, M., Tielbörger, K., Tomiolo, S., 2022. Effects of plastic fragments on plant performance are mediated by soil properties and drought. Sci. Rep. 12, 17771. https://doi.org/10.1038/s41598-022-22270-5.

Lwanga, E.H., Beriot, N., Corradini, F., Silva, V., Yang, X., Baartman, J., et al., 2022. Review of microplastic sources, transport pathways and correlations with other soil stressors: a journey from agricultural sites into the environment. Chemical and Biological Technologies in Agriculture 9, 20. https://doi.org/10.1186/s40538-021-00278-9.

Meng, F., Yang, X., Riksen, M., Xu, M., Geissen, V., 2021. Response of common bean (Phaseolus vulgaris L.) growth to soil contaminated with microplastics. Sci. Total Environ. 755, 142516 https://doi.org/10.1016/j.scitotenv.2020.142516.

Munz, M., Kreiß, J., Krüger, L., Schmidt, L.K., Bochow, M., Bednarz, M., et al., 2023a. Application of high-resolution near-infrared imaging spectroscopy to detect microplastic particles in different environmental compartments. Water Air Soil Pollut. 234, 286. https://doi.org/10.1007/s11270-023-06245-4.

Munz, M., Loui, C., Postler, D., Pittroff, M., Oswald, S.E., 2023b. Transport and retention of micro-polystyrene in coarse riverbed sediments: effects of flow velocity, particle and sediment sizes. Microplastics and Nanoplastics (in revision).

Prata, J.C., da Costa, J.P., Duarte, A.C., Rocha-Santos, T., 2019. Methods for sampling and detection of microplastics in water and sediment: a critical review. TrAC Trends Anal. Chem. 110, 150–159. https://doi.org/10.1016/j.trac.2018.10.029.

Qi, Y., Yang, X., Pelaez, A.M., Huerta Lwanga, E., Beriot, N., Gertsen, H., Garbeva, P., Geissen, V., 2018. Macro- and micro- plastics in soil-plant system: Effects of plastic mulch film residues on wheat (Triticum aestivum) growth. Sci. Total Environ. 1048–1056. https://doi.org/10.1016/j.scitotenv.2018.11.123.

Rillig, M.C., Lehmann, A., 2020. Microplastic in terrestrial ecosystems. Science 368, 1430–1431. https://doi.org/10.1126/science.abb5979.

Rillig, M.C., Ziersch, L., Hempel, S., 2017. Microplastic transport in soil by earthworms. Sci. Rep. 7, 1362. https://doi.org/10.1038/s41598-017-01594-7.

Rillig, M.C., Lehmann, A., Ryo, M., Bergmann, J., 2019. Shaping up: toward considering the shape and form of pollutants. Environ. Sci. Technol. 53, 7925–7926. https://doi.org/10.1021/acs.est.9b03520.

Rochman, C.M., 2018. Microplastics research—from sink to source. Science 360, 28–29. https://doi.org/10.1126/science.aar7734.

Roubin, E., Andò, E., Roux, S., 2019. The colours of concrete as seen by X-rays and neutrons. Cem. Concr. Compos. 104, 103336 https://doi.org/10.1016/j.cemconcomp.2019.103336.

Stamati, O., Andò, E., Roubin, E., Cailletaud, R., Wiebicke, M., Pinzon, G., et al., 2020. Spam: software for practical analysis of materials. Journal of Open Source Software 5. https://doi.org/10.21105/joss.02286.

Tang, Y., Liu, Y., Chen, Y., Zhang, W., Zhao, J., He, S., et al., 2021. A review: research progress on microplastic pollutants in aquatic environments. Sci. Total Environ. 766, 142572 https://doi.org/10.1016/j.scitotenv.2020.142572.

Tengattini, A., Lenoir, N., Andò, E., Giroud, B., Atkins, D., Beaucour, J., et al., 2020. NeXT-Grenoble, the neutron and X-ray tomograph in Grenoble. Nucl. Instrum. Methods Phys. Res., Sect. A 968, 163939. https://doi.org/10.1016/j.nima.2020.163939.

Tötzke, C., Kardjilov, N., Manke, I., Oswald, S.E., 2017. Capturing 3D water flow in rooted soil by ultra-fast neutron tomography. Sci. Rep. 7, 6192. https://doi.org/10.1038/s41598-017-06046-w.

Tötzke, C., Kardjilov, N., Lenoir, N., Manke, I., Oswald, S.E., Tengattini, A., 2019. What comes NeXT? High-speed neutron tomography at ILL. Opt. Express 27, 28640–28648. https://doi.org/10.1364/OE.27.028640.

Tötzke, C., Kardjilov, N., Hilger, A., Rudolph-Mohr, N., Manke, I., Oswald, S.E., 2021a. Three-dimensional in vivo analysis of water uptake and translocation in maize roots by fast neutron tomography. Sci. Rep. 11, 10578. https://doi.org/10.1038/s41598-021-90062-4.

Tötzke, C., Oswald, S.E., Hilger, A., Kardjilov, N., 2021b. Non-invasive detection and localization of microplastic particles in a sandy sediment by complementary neutron and X-ray tomography. J. Soil. Sediment. 21, 1476–1487. https://doi.org/10.1007/s11368-021-02882-6.

Wan, Y., Wu, C., Xue, Q., Hui, X., 2019. Effects of plastic contamination on water evaporation and desiccation cracking in soil. Sci. Total Environ. 654, 576–582. https://doi.org/10.1016/j.scitotenv.2018.11.123.

Wang, Z., Li, W., Li, W., Yang, W., Jing, S., 2023. Effects of microplastics on the water characteristic curve of soils with different textures. Chemosphere 317, 137762. https://doi.org/10.1016/j.chemosphere.2023.137762.

Weber, C.J., Lechthaler, S., 2021. Plastics as a stratigraphic marker in fluvial deposits. Anthropocene 36, 100314. https://doi.org/10.1016/j.ancene.2021.100314.

Weber, C.J., Santowski, A., Chifflard, P., 2022. Investigating the dispersal of macro- and microplastics on agricultural fields 30 years after sewage sludge application. Sci. Rep. 12, 6401. https://doi.org/10.1038/s41598-022-10294-w.

Xu, B., Liu, F., Cryder, Z., Huang, D., Lu, Z., He, Y., et al., 2020. Microplastics in the soil environment: occurrence, risks, interactions and fate – a review. Crit. Rev. Environ. Sci. Technol. 50, 2175–2222. https://doi.org/10.1080/10643389.2019.1694822.

Yu, Y., Flury, M., 2021. Current understanding of subsurface transport of micro- and nanoplastics in soil. Vadose Zone J. 20, e20108 https://doi.org/10.1002/vzj2.20108.

Yu, Y., Battu, A.K., Varga, T., Denny, A.C., Zahid, T.M., Chowdhury, I., et al., 2023. Minimal impacts of microplastics on soil physical properties under environmentally relevant concentrations. Environ. Sci. Technol. 57, 5296–5304. https://doi.org/10.1021/acs.est.2c09822.